



This discussion paper is/has been under review for the journal Atmospheric Measurement Techniques (AMT). Please refer to the corresponding final paper in AMT if available.

# A new method of measuring aerosol optical properties from digital twilight photographs

M. Saito and H. Iwabuchi

Center for Atmospheric and Oceanic Studies, Graduate School of Science, Tohoku University,  
6-3 Aoba Aramaki-aza, Sendai, Miyagi 980-8578, Japan

Received: 19 October 2014 – Accepted: 1 December 2014 – Published: 6 January 2015

Correspondence to: M. Saito (masanori@caos-a.geophys.tohoku.ac.jp)

Published by Copernicus Publications on behalf of the European Geosciences Union.

**A new method of measuring aerosol optical properties from digital twilight photographs**

M. Saito and H. Iwabuchi

Title Page

Abstract

Introduction

Conclusions

References

Tables

Figures



Back

Close

Full Screen / Esc

Printer-friendly Version

Interactive Discussion



## Abstract

An optimal-estimation algorithm for inferring aerosol optical properties from digital twilight photographs is proposed. The sensitivity of atmospheric components and surface characteristics to brightness and color of twilight sky is investigated, and the results suggest that tropospheric and stratospheric aerosol optical thickness (AOT) are sensitive to condition of the twilight sky. The coarse–fine particle volume ratio is moderately sensitive to the sky condition near the horizon under a clean-atmosphere condition. A radiative transfer model that takes into account a spherical-shell atmosphere, refraction, and multiple scattering is used as a forward model. Error analysis shows that the tropospheric and stratospheric AOT can be retrieved without significant bias. Comparisons with results from other ground-based instruments exhibit reasonable agreement on AOT. A case study suggests that the AOT retrieval method can be applied to atmospheric conditions with varying aerosol vertical profiles and vertically inhomogeneous species in the troposphere.

## 1 Introduction

Twilight sky, one of the most beautiful sights in our daily life, varies from day to day. The color of the sky under clear-sky conditions gradates from orange-red and salmon red near the horizon to blue-gray and blue at zenith. This gradation results from Rayleigh scattering caused by molecules (Minnaert, 1993). Twilight sky has been studied for more than a half century, elucidating the effects of ozone and stratospheric aerosol on twilight sky colors. As an example, ozone has the Chappuis band, an absorption band with a peak wavelength of about 550 to 600 nm. Hulburt (1953) simulated twilight-sky brightness at zenith with a radiative transfer model (RTM) based on the Rayleigh scattering theory and taking into account ozone absorption. Hulburt's results showed that the contribution of ozone absorption is more important than that of Rayleigh scattering in providing the blue color at zenith. Lee et al. (2011) measured twilight sky in Antarc-

AMTD

8, 191–234, 2015

## A new method of measuring aerosol optical properties from digital twilight photographs

M. Saito and H. Iwabuchi

Title Page

Abstract

Introduction

Conclusions

References

Tables

Figures

◀

▶

◀

▶

Back

Close

Full Screen / Esc

Printer-friendly Version

Interactive Discussion





## A new method of measuring aerosol optical properties from digital twilight photographs

M. Saito and H. Iwabuchi

Title Page

Abstract

Introduction

Conclusions

References

Tables

Figures

◀

▶

◀

▶

Back

Close

Full Screen / Esc

Printer-friendly Version

Interactive Discussion



of 700 nm at zenith. Mateshvili et al. (2013) developed a method that uses optimal estimation to infer the upper tropospheric and stratospheric aerosol vertical profiles from spectral at zenith during twilight, providing stratospheric AOT both pre- and post-eruption of the volcano Nabro. The aerosol information obtained from these twilight measurements was consistent with that from other measurements, showing that twilight sky measurement is a useful tool for gathering information on aerosols.

It is well known that tropospheric and stratospheric aerosol contributes to climate change. The optical and radiative properties of aerosol can vary strongly according to relative amount, chemical components, and particle sizes. This results in high uncertainty of climate change prediction in terms of radiation budget (IPCC, 2013). Aerosol measurement is carried out with satellite- and ground-based instruments such as the moderate-resolution imaging spectroradiometer (MODIS) devices on-board the Terra and Aqua satellites and the aerosol robotic network (AERONET) system. This provide on solar and sky measurements (Remer et al., 2005; Holben et al., 1998). However, most of the instruments useful for aerosol measurement require passive remote-sensing techniques, meaning that these instruments cannot infer aerosol properties in regions without direct sunlight. In addition, satellite-based instruments with passive sensors cannot infer aerosol properties in deserts and snow-covered regions because of high surface reflectivity. Particularly in the polar region during winter, aerosol measurements and their data are very limited because of the length of the polar night (sunless condition in all day). In the region, a few measurements are carried out by active remote sensing techniques, in situ sampling, and difficult aerosol measurements that use direct light from the moon and stars as a substitute for direct sunlight transmittance methods (Heber et al., 2002; Berkoff et al., 2011).

Recently, digital cameras have begun to be used as measurement instruments (e.g., Lee and Andres, 2003; Lee et al., 2011). Ehrlich et al. (2011) provided a method for constructing a bi-directional reflectance distribution function for cloud from data obtained by a digital single-lens reflex (DSLR) camera installed on an airplane. Kataoka et al. (2013) developed a method for estimating the altitude of visible aurorae from





enable comparison between the values, the values of  $u'_{k,i}$  are normalized by the photon flux density convert radiance-proportional RAW counts  $u_{k,i}$ , and  $u_{k,i}$ , which can be defined as

$$u_{k,i} = \int_0^{\infty} S_k(\lambda) I_i(\lambda) d\lambda, \quad (1)$$

5 where the function  $S_k(\lambda)$  is the relative CMF. The optimal estimation-based inverse calculation is applied to Eq. (1), yielding determining  $S_k(\lambda)$  with some associated uncertainty. In this experiment, the same camera configurations are used for all photographic observations, and an exposure time of 8 s is used. The CMFs for the Nikon D200, as determined by Sigarnes et al. (2008), are used as prior information. The vignetting characteristics of the fisheye lens have been investigated by Saito and Iwabuchi (2015), and we eliminate the effects of vignetting from the camera RAW counts. Figure 2 shows the relative CMFs of the Nikon D7000. The center wavelength of each channel (i.e., the most sensitive wavelength) is shifted to a shorter wavelength, by about 10 nm for R channel and 20 nm for the B channel, relative to those of the Nikon D200. Moreover, the shape of the spectral sensitivity on the G channel of the D7000 is broader in shape than that of the D200.

For photographic observation in twilight, the RAW counts  $u'_{k,i}$  are converted to radiance-proportional RAW counts  $u_k$ , which can be rewritten as  $c/I_k$ , where  $I_k$  is channel-averaged spectral radiance, weighted by the camera spectral response of the channel  $k$ , and  $c$  is a parameter determined by the quantum efficiency of the CMOS and the ISO film speed. Finally, the chromaticity (R/G, B/G) is obtained by dividing each of  $c/I_R$  and  $c/I_B$  by  $c/I_G$ , and the normalized brightness  $G_n$  is obtained by dividing the value of  $c/I_G$  by the value of  $c/I_G$  measured at VZA of  $70^\circ$  and RAA of  $0^\circ$  for all VZAs, SZAs, and RAAs in the twilight sky. This process results in an 840-dimensional measurement for each photographic observation. For prior knowledge, this method requires only the relative CMFs of the camera; absolute calibration is unnecessary because the

## A new method of measuring aerosol optical properties from digital twilight photographs

M. Saito and H. Iwabuchi

Title Page

Abstract

Introduction

Conclusions

References

Tables

Figures

◀

▶

◀

▶

Back

Close

Full Screen / Esc

Printer-friendly Version

Interactive Discussion





aerosol  $b_{\text{up}}(z)$ , each of which follows a Gamma distribution. The shape and scale parameters for each aerosol vertical profile are summarized in Table 3. By substitution, the tropospheric aerosol vertical profile  $b_{\text{tr}}(z)$  can be written as

$$b_{\text{tr}}(z) = a_{\text{bg}}b_{\text{bg}}(z) + a_{\text{bl}}b_{\text{bl}}(z) + a_{\text{up}}b_{\text{up}}(z), \quad (3)$$

5 where  $a_{\text{bg}}$ ,  $a_{\text{bl}}$ , and  $a_{\text{up}}$  are, respectively, the AOT fraction of background aerosol, boundary layer aerosol, and upper tropospheric aerosol relative to total tropospheric AOT at a wavelength of 550 nm. In this study, the AOT fractions are assumed to be in the proportions  $a_{\text{bg}} : a_{\text{bl}} : a_{\text{up}} = 1 : 1.2 : 0.4$ . In general, the extinction coefficient in the middle-upper troposphere shrinks exponentially with increasing altitude, and aerosol is  
 10 abundant in the boundary layer. The extinction coefficients  $\beta(z)$  can be calculated by multiplying the AOTs by  $b(z)$ .

The distribution of aerosol particle volumes  $dV/dr$  is assumed to follow a lognormal distribution:

$$\frac{dV}{dr} = \frac{V_{0,\text{F}}}{r\sqrt{2\pi}\ln s_{\text{F}}} \exp\left[-\frac{1}{2}\left(\frac{\ln r - \ln r_{\text{mod},\text{F}}}{\ln s_{\text{F}}}\right)^2\right] + \frac{V_{0,\text{C}}}{r\sqrt{2\pi}\ln s_{\text{C}}} \exp\left[-\frac{1}{2}\left(\frac{\ln r - \ln r_{\text{mod},\text{C}}}{\ln s_{\text{C}}}\right)^2\right]. \quad (4)$$

15 Here,  $r$  is particle radius, and  $r_{\text{mod}}$ ,  $s$ , and  $V_0$  are the mode radius, geometrical SD, and particle volume, respectively, with subscript F indicating fine particle mode and subscript C indicating coarse particle mode. The parameters  $r_{\text{mod}}$  and  $s$  for this aerosol model are taken from the rural aerosol model proposed by Hänel (1976). To simplify for aerosol properties representation, this paper introduces the coarse–fine particle  
 20 volume ratio  $\zeta$ , defined as

$$\zeta = \frac{V_{0,\text{C}}}{V_{0,\text{F}}}. \quad (5)$$

**A new method of measuring aerosol optical properties from digital twilight photographs**

M. Saito and H. Iwabuchi

Title Page	
Abstract	Introduction
Conclusions	References
Tables	Figures
◀	▶
◀	▶
Back	Close
Full Screen / Esc	
Printer-friendly Version	
Interactive Discussion	



From the above model setting, the spectral radiance-integrated RGB signals can be calculated by multiplying the simulated spectral radiance of twilight sky with the camera CMFs. The normalized brightness  $G_n$  and the chromaticity (R/G, B/G) can then be obtained in the way described in Sect. 2.

### 3.2 Sensitivity tests

The sensitivities of the chromaticity and normalized brightness in twilight sky to tropospheric AOT  $\tau_{tr}$ , stratospheric AOT  $\tau_{st}$ , coarse–fine particle volume ratio  $\zeta$ , and other atmosphere–surface characteristics were tested. For the sensitivity tests, the complex refractive indices of aerosol were assumed to be 1.5 for the real part and 0.01 for the imaginary part. The results are described in Figs. 3, 4, and 5. In the twilight sky, and particularly near the horizon, as  $\tau_{tr}$  increases,  $G_n$  and R/G decrease and B/G increases (Fig. 3a and b). These relations suggest that the twilight sky becomes dark and blue near the horizon, which is consistent with the results of Saito et al. (2013). Figure 3c and d shows the sensitivities of the twilight sky to  $\tau_{st}$ . With large  $\tau_{st}$ , the value of  $G_n$  at VZAs of 75–85° increases and all R/G (resp., B/G) values increase (decrease), so that the reddened twilight glow is represented. These results are consistent with several reports on the very intense twilight glow (the so-called twilight phenomenon) that results from volcanic aerosol injection into the stratosphere by volcanic eruptions (Volz, 1964, 1965). The sensitivity tests show that R/G increases under high  $\zeta$  conditions only near the horizon (Fig. 3e and f). Figure 4 shows the sensitivities of the brightness and the chromaticity in twilight glow with VZA of 85°, SZA of 93°, and RAA of 0°. In the R/G– $G_n$  cross-section (Fig. 4b),  $G_n$  depends strongly and inversely on  $\tau_{tr}$ , decreasing under typical aerosol property condition ( $\zeta = 1$ ) as  $\tau_{tr}$  increases. In contrast, for R/G, sensitivity to  $\tau_{st}$  predominates, and R/G increases with large  $\tau_{st}$  (Fig. 4b). The sensitivities of twilight glow are sufficient for modeling with  $\tau_{tr}$  in 0.01–0.5 and  $\tau_{st}$  in 0.002–0.1, while the chromaticity and normalized brightness in this sector are less sensitive to  $\zeta$  (Fig. 4c and d). Figure 5 is the same as Fig. 4 except near the horizon with VZA of 88°, SZA of 91°, and RAA of 0°. The sensitivity of the twilight sky to  $\tau_{st}$  and

## A new method of measuring aerosol optical properties from digital twilight photographs

M. Saito and H. Iwabuchi

Title Page

Abstract

Introduction

Conclusions

References

Tables

Figures

◀

▶

◀

▶

Back

Close

Full Screen / Esc

Printer-friendly Version

Interactive Discussion



## A new method of measuring aerosol optical properties from digital twilight photographs

M. Saito and H. Iwabuchi

Title Page

Abstract

Introduction

Conclusions

References

Tables

Figures

◀

▶

◀

▶

Back

Close

Full Screen / Esc

Printer-friendly Version

Interactive Discussion



$\zeta$  is weak for  $\tau_{tr} = 0.13$  (Fig. 5a and b). Figure 5c and d suggests that the sky is more sensitive to  $\zeta$  when  $\tau_{tr}$  is smaller. In such cases, R/G and  $G_n$  increase with increasing  $\zeta$ . As above, twilight sky is sensitive to  $\zeta$  in the range of 0.2 to 5 under the clean atmospheric condition ( $\tau_{tr} \lesssim 0.1$ ). To summarize this section, the sensitivity tests showed that the normalized brightness and the chromaticity in the twilight sky have sufficient sensitivity to tropospheric and stratospheric AOT and have moderate sensitivity to the coarse–fine particle volume ratio under small AOT conditions.

The sensitivity to other atmospheric and surface characteristics was investigated, with the results showing that the sensitivity to ozone column of twilight sky color is moderate, as previously shown by Hulburt (1953). However, the sensitivities of sky brightness and color to surface albedo, refractive indices, and water vapor column were found to be very weak (not shown).

### 3.3 Model setup for aerosol retrievals

To apply the JACOSPAR RTM to the forward model for aerosol retrieval, we refined the RTM to allow faster computation by semi-analytically calculating singly scattered light and then linearly interpolating multiply scattered light from a lookup table (LUT), which was pre-calculated by the BMC method. Ozone column amount data were taken with the ozone monitoring instruments (OMI) onboard the Aura satellite and considered in the atmospheric model and in the LUT of the RTM. We assumed that other surface–atmospheric conditions (such as: surface albedo, water vapor, and refractive indices) agreed with climatic values.

## 4 Retrieval method and error analysis

### 4.1 The retrieval method

The retrieval method is a maximum a posteriori (MAP) estimation method based on optimal estimation (Rodgers, 2000). This method derives an optimal solution from mea-

surement data under the constraints of prior information, and is presently in use for aerosol and cloud optical property remote sensing (e.g., Watts et al., 2011; Mateshvili et al., 2013; Iwabuchi et al., 2014). A measurement vector  $\mathbf{y}$  derived from twilight photographs, a state vector  $\mathbf{x}$  that includes aerosol optical properties as elements, and a set of model parameters  $\boldsymbol{\rho}$  are defined as

$$\mathbf{x} = \begin{pmatrix} \ln \tau_{\text{tr}} \\ \ln \tau_{\text{st}} \\ \ln \zeta \end{pmatrix}, \quad (6)$$

$$\mathbf{y} = \begin{pmatrix} y_1 \\ y_2 \\ \vdots \\ y_n \end{pmatrix}, \quad (7)$$

$$\boldsymbol{\rho} = \begin{pmatrix} \omega_{\text{H}_2\text{O}} \\ \omega_{\text{O}_3} \\ \alpha \\ m_r \\ m_i \end{pmatrix}, \quad (8)$$

where  $\omega_{\text{H}_2\text{O}}$  is column water vapor amount,  $\omega_{\text{O}_3}$  is column ozone amount,  $\alpha$  is surface albedo, and  $m_r$  and  $m_i$  are the real and imaginary parts, respectively, of the refractive indices of aerosol. The number of measurement vector elements  $n$  is set at 840 because the number is defined as the number of measurement elements multiplied by the number of measurement directions (3 of measurement elements and 280 of measurement directions, which result from 10 VZAs, 7 SZAs, and 4 RAAs). We can formally describe the physics as the forward model function  $f(\mathbf{x})$ :

$$\mathbf{y} = f(\mathbf{x}, \boldsymbol{\rho}) + \mathbf{e}, \quad (9)$$

**A new method of measuring aerosol optical properties from digital twilight photographs**

M. Saito and H. Iwabuchi

Title Page	
Abstract	Introduction
Conclusions	References
Tables	Figures
◀	▶
◀	▶
Back	Close
Full Screen / Esc	
Printer-friendly Version	
Interactive Discussion	



where  $\mathbf{e}$  is the measurement–model error vector. The cost function  $J(\mathbf{x})$  can be described as

$$J(\mathbf{x}) = (\mathbf{x} - \mathbf{x}_a)^T \mathbf{S}_a^{-1} (\mathbf{x} - \mathbf{x}_a) + [\mathbf{y} - f(\mathbf{x}, \boldsymbol{\rho})]^T \mathbf{S}_y^{-1} [\mathbf{y} - f(\mathbf{x}, \boldsymbol{\rho})], \quad (10)$$

where  $\mathbf{x}_a$  is an a priori state vector,  $\mathbf{S}_a$  is an a priori state error covariance matrix, and  $\mathbf{S}_y$  is a measurement–model error covariance matrix. The derivation of  $\mathbf{S}_y$  will be described in Sect. 4.2. We summarize the a priori state and its error variance in Table 4. The assumed  $\mathbf{S}_a$  is a diagonal matrix, with the main diagonal taken as a vector of error variances from prior information. The prior state and its geometrical SD for  $\tau_{\text{tr}}$  are assumed to be 0.13 and 1.19, respectively, which is taken from the values in Dubovik et al. (2002) for AOTs in urban, continental, and desert regions, which range from 0.04 to 0.43, as found from ground-based observations. The a priori value of  $\tau_{\text{st}}$  is set to be 0.005 with a geometrical SD of 1.15 (Hess et al., 1998). The a priori value for  $\zeta$  is assumed to be that of a rural aerosol model with a bimodal distribution of particle volume, as proposed by Hänel (1976). The geometrical SDs for the prior information are set to be large value to avoid overfitting of the state vector  $\mathbf{x}$ , which has components  $\ln \tau_{\text{tr}}$ ,  $\ln \tau_{\text{st}}$ , and  $\ln \zeta$ . When the state vector becomes optimal, the cost function should be below the degrees of freedom of the measurement vector (Rodgers, 2000). Therefore, an optimal state  $\mathbf{x}_{\text{opt}}$  gives

$$J(\mathbf{x}_{\text{opt}}) \approx n. \quad (11)$$

Because the measurement vector calculated according to the forward model is nonlinearly dependent on the state vector, we apply the Levenberg–Marquardt method (LMM) to solve the inverse problem. The LMM can provide a stable solution for moderately nonlinear problems (Rodgers, 2000). The method is iteratively applied to find an optimal solution for  $\mathbf{x}$ . The state vector at the  $i + 1$ th iteration,  $\mathbf{x}_{i+1}$ , is given by

$$\mathbf{x}_{i+1} = \mathbf{x}_i + [(1 + \gamma) \mathbf{S}_a^{-1} + \mathbf{K}_i^T \mathbf{S}_y^{-1} \mathbf{K}_i]^{-1} \left\{ \mathbf{K}_i^T \mathbf{S}_y^{-1} [\mathbf{y} - f(\mathbf{x}, \boldsymbol{\rho})] - \mathbf{S}_a^{-1} [\mathbf{x} - \mathbf{x}_a] \right\}, \quad (12)$$

**A new method of measuring aerosol optical properties from digital twilight photographs**

M. Saito and H. Iwabuchi

Discussion Paper | Discussion Paper | Discussion Paper | Discussion Paper | Discussion Paper

Title Page

Abstract

Introduction

Conclusions

References

Tables

Figures

◀

▶

◀

▶

Back

Close

Full Screen / Esc

Printer-friendly Version

Interactive Discussion





**A new method of measuring aerosol optical properties from digital twilight photographs**

M. Saito and H. Iwabuchi

Title Page

Abstract

Introduction

Conclusions

References

Tables

Figures

◀

▶

◀

▶

Back

Close

Full Screen / Esc

Printer-friendly Version

Interactive Discussion



Sendai, Japan, as obtained by ground-based measurements (1.44–1.57 real part and 0.007–0.057 imaginary part). The surface albedo  $\alpha$  is assumed to be 0.1 because of the annual variation of  $\alpha$  from 0.05 to 0.3, which was found by Zhou et al. (2003).

The forward model error originates from uncertainties about the particle size distribution, from the vertical profile shape assumed in the forward model, and also includes a smoothing error resulting from linear interpolation in the LUT. The forward model error is evaluated by adding Gaussian random noise to the parameters for aerosol particle size distribution and vertical profile shape (specifically, to the mode radii for the volume particle size distributions, and to the scale and shape parameters of the Gamma distributions for the vertical profile) and running the forward model and JACOSPAR RTM for perturbed sets of model-assumed parameters and finally calculating the difference between each model's output. The results from JACOSPAR RTM are taken as ground truth data. The dependence of assumption errors in the forward model on the measurement angles is shown in Fig. 6. The root-mean-square (RMS) errors of the chromaticity and the normalized brightness are consistently larger with larger SZAs and are smaller with smaller VZAs and RAAs. The RMS errors are in the range 1–3 % for R/G, 3–5 % for B/G, and 5–10 % for  $G_n$ .

The model parameter errors are evaluated by adding Gaussian random noise to the model parameters shown in Table 5 and running the forward model for perturbed sets of model parameters. We show the dependence of the model parameter errors on the measurement angles in Fig. 7. The chromaticity errors depend weakly on the value of RAA and SZA and are moderately larger with larger values of VZA. In contrast, the error in  $G_n$  rapidly increases with increasing SZA and is slightly larger with smaller values of RAA and larger values of VZA. The RMS errors for R/G and B/G are in the range 3–5 %. The RMS error for  $G_n$  is below 5 % for SZA of 90–94°, but in the range 20–80 % for SZA of 95–96°. The model parameter errors are the largest errors and are dominant in the model–measurement error. The covariance matrices for errors in the forward model assumptions and the model parameters are taken as constant matrices for the aerosol retrievals in this study. The applied algorithm could be improved by accounting for the

effects of the state vector and model parameter values on these matrices. This is left for future work.

The measurement errors include CMOS noise and biases, uncertainties in the inferred camera response functions, camera-orientation errors, and time-lag error during taking the photographs. CMOS biases can arise from exposure time, aperture, and temperature. CMOS noise errors for each angle are determined by the variance of RAW counts among pixels taken from the corresponding angles. The time-lag error is assumed to be normally distributed with SD 5 s, which gives an uncertainty of  $\sim 0.015^\circ$  for SZA, and the camera-orientation error is assumed to be normally distributed with SD  $0.5^\circ$  for VZA and  $0.3^\circ$  for RAA. Further, the errors are estimated by running the forward model with Gaussian random noise perturbation of the camera angles. As a result, the CMOS noise is on the order of 3 to 5%, and other errors are very small at all angles, on the order of 0.5 to 1% for the chromaticity and normalized brightness.

### 4.3 Retrieval-error analysis

The errors in retrieved aerosol properties originate from the measurement–model error and the sensitivity of the state vector of the sky to atmospheric conditions. For the error sources in Table 3, the retrieval error is evaluated by retrieval simulations. First, after assuming a state  $\mathbf{x}$  and model parameters  $\mathbf{p}_{\text{noise}}$  and adding Gaussian random noise, the forward-model-simulated measurements  $\mathbf{y}_{\text{noise}}$  are calculated, and Gaussian random noise is added to simulate measurement error and the forward model error. Second, we try to retrieve the state vector  $\mathbf{x}_{\text{noise}}$  from  $\mathbf{y}_{\text{noise}}$  with this algorithm. Finally, the truth–retrieval difference  $\mathbf{x}_{\text{noise}} - \mathbf{x}$  is obtained. Each state was simulated 100 times and the retrieval error was taken as the average error. The retrieval results with filtering ( $J(\mathbf{x}) < 1000$ ) are shown in Fig. 8. The value of  $\tau_{\text{tr}}$  is almost correctly retrieved, with RMS error of 0.14% and a slightly negative bias ( $\sim 5\%$ ) in the range of 0.01–0.5 (Fig. 8a). The retrieval uncertainty is very small under the clean and moderately turbid atmospheric conditions for  $\tau_{\text{tr}}$  from 0.01 to 0.3, suggesting that this method can retrieve tropospheric AOTs with high precision. In the more turbid atmospheric

## A new method of measuring aerosol optical properties from digital twilight photographs

M. Saito and H. Iwabuchi

Title Page

Abstract

Introduction

Conclusions

References

Tables

Figures

◀

▶

◀

▶

Back

Close

Full Screen / Esc

Printer-friendly Version

Interactive Discussion



## A new method of measuring aerosol optical properties from digital twilight photographs

M. Saito and H. Iwabuchi

Title Page

Abstract

Introduction

Conclusions

References

Tables

Figures

◀

▶

◀

▶

Back

Close

Full Screen / Esc

Printer-friendly Version

Interactive Discussion



conditions ( $\tau_{tr} > 0.3$ ), the uncertainty in the retrieved  $\tau_{tr}$  is around  $\pm 0.1$ . The value of  $\tau_{st}$  is also correctly retrieved with a RMS error of 2.4% and no notable bias (Fig. 8b). The retrieved value of  $\tau_{st}$  is overestimated under small tropospheric AOT conditions as a result of the particular characteristics of this retrieval method (not shown). The uncertainties for  $\tau_{st}$  retrieval are small for large values of  $\tau_{st}$  and are slightly larger for small values of  $\tau_{st}$ , suggesting that the value of  $\tau_{st}$  can be retrieved accurately under the dense  $\tau_{st}$  conditions caused by volcanic eruption, such as the Mt. Pinatubo eruption in 1991. Figure 8c shows that the value of  $\zeta$  can be retrieved when it is in the range of 1 to 5 and there is a clean atmospheric conditions ( $\tau_{tr} \sim 0.1$ ). In this case (blue marks in the figure), the RMS error is somewhat large (18.2%). Additionally, the retrieved values of  $\zeta$  are scattered, centered mostly around the a priori assumption under moderate and dense aerosol conditions ( $\tau_{tr} > 0.13$ ). This occurs because the sensitivity of  $\zeta$  on twilight sky is weak with large tropospheric AOTs, as shown in Sect. 3.2. When small particles dominate ( $\zeta < 1$ ), the retrieved values of  $\zeta$  are almost equal to the a priori assumption. Figure 8d shows the retrieved  $\zeta$  with the retrieval method for fixed and given truth  $\tau_{st}$  values. The RMS error in the  $\zeta$  retrievals is smaller (at 13.3%) than that for retrievals under non-fixed  $\tau_{st}$  values regardless, and this is independent of  $\tau_{tr}$  in the range 0.01–0.5. This suggests that the accuracy of the  $\zeta$  retrievals can be improved if the  $\tau_{st}$  is accurately known from other instruments. Furthermore, no dependence of retrieved  $\zeta$  on stratospheric AOTs is found, suggesting that the slightly large RMS error in the  $\zeta$  retrievals might result from error in retrieving  $\tau_{st}$ . In addition, the degrees of freedom for the signals obtained from the measurements are around 3 in most cases, showing that the measurement data are sufficient for retrievals by this method.



$\zeta$  retrieved from the camera are compared with those calculated from particle volume distributions retrieved from the skyradiometer (Fig. 9c). The retrieved value of  $\zeta$  tends to be close to the a priori assumption for moderate and large AOTs ( $\tau_{\text{tr}} > 0.13$ ) and vary widely for small AOTs ( $\tau_{\text{tr}} < 0.13$ ). This disparity results from the weak correlation between the camera and the skyradiometer.

## 5.2 Case studies

To test the flexibility under various aerosol conditions (e.g., vertical profiles and aerosol species) of this retrieval method, we chose three characteristic cases and analyzed the simulation results in detail with respect to the vertical profiles of the aerosol extinction coefficients. Figure 10 shows photographs of the twilight sky taken on (a) 31 January 2013, (b) 23 May 2013, and (c) 3 June 2013. These photographs were taken at an SZA of  $94^\circ$ . In Fig. 10a, a bright red-orange twilight glow is seen near the horizon, and the twilight sky color gradates from orange to blue. The brightness rapidly decreases as the VZA decreases. In contrast, the color in Fig. 10b seems to be dull across the sky in comparison with Fig. 10a. An orange-to-gray twilight glow is present above a dark-blue segment that appears near the horizon (Saito et al., 2013). In Fig. 10c, the range of the twilight sky color is the smallest among the three cases, and a dark-blue segment can be seen near the horizon, similar to that in Fig. 10b. Figure 11 shows the vertical profiles of aerosol extinction coefficients in the troposphere from the ground to an altitude of 6 km; these are derived from the lidar measurements for each case (Shimizu et al., 2010). In the lidar products, the lidar ratio of 50 sr is assumed, and the inferred extinction coefficients are separated into spherical and non-spherical particles.

Table 6 summarizes the results from the ground-based observations (the sunphotometer and the skyradiometer, collocated at the photographic observation site) and from the daily means of aerosol optical properties, as calculated by the aerosol transport model SPRINTARS (Takemura et al., 2000, 2002, 2005). The sunphotometer measures direct solar light in the visible to near infrared wavelengths to infer the AOTs. For 31 January 2013 (case a), very clean atmosphere with an AOT of 0.02–0.03 is

### A new method of measuring aerosol optical properties from digital twilight photographs

M. Saito and H. Iwabuchi

Title Page

Abstract

Introduction

Conclusions

References

Tables

Figures

◀

▶

◀

▶

Back

Close

Full Screen / Esc

Printer-friendly Version

Interactive Discussion



## A new method of measuring aerosol optical properties from digital twilight photographs

M. Saito and H. Iwabuchi

Title Page

Abstract

Introduction

Conclusions

References

Tables

Figures

◀

▶

◀

▶

Back

Close

Full Screen / Esc

Printer-friendly Version

Interactive Discussion



simulated by the SPRINTARS and weak backscatter signals are obtained from lidar measurement. Moreover, spherical particles are dominant in this case. In contrast, the SPRINTARS products suggest that sulphate and dust particles were transported from the eastern part of continental China to Japan from 20 to 26 May 2013. Consistently, the lidar measurements show the presence of nonspherical particles at altitudes of 3–6 km and the presence of spherical/nonspherical mixed particles in the boundary layer for 23 May 2013 (case b). For 3 June 2013 (case c), dust transported from the north inland area of China to Japan from 2 to 5 June 2013 is shown by the model. A spherical/nonspherical mixture of particles is present in the boundary layer (altitudes of 0–2 km), and nonspherical particles are dominant above 6 km, according to the lidar measurements.

From the above results, the atmospheric characteristics are clean atmosphere in case (a), dust-pollutant mixed particles transported from eastern China in case (b), and yellow sand transported from inland China in case (c). Additionally, the vertical profiles and aerosol species are vertically inhomogeneous in cases (b) and (c). A comparison of the results retrieved from the photographic observations with the corresponding results from other products shows that the retrieved AOTs are reasonable for cases (a) and (b), with AOTs of  $0.074 \pm 0.012$  (a) and  $0.101 \pm 0.006$  (b) relative to estimates from other ground-based passive instruments. The retrieved values of  $\zeta$  are  $2.86 \pm 0.34$  (a) and  $0.98 \pm 0.07$  (b). For case (c), an AOT of  $0.251 \pm 0.006$  is inferred from the camera, which is slightly lower than the AOT obtained from other products. The main reason for this is that the inferred  $\tau_{tr}$  is negatively biased at larger AOTs due to the characteristics of the present method. Additionally, it might be that the temporal–spatial variability of aerosol optical properties under dust events affects the bias. Specifically, during dust events, aerosol optical properties showed high variability, and so they varied more widely during the time-lag between camera observations and other measurements than they did in the other cases, resulting in the difference in AOT. The retrieved value of  $\zeta$  is eliminated in the case (c) because of low confidence in the  $\zeta$  retrieval, which was predicted by the retrieval error analysis (Sect. 4.3) for large AOT conditions. The AOTs



**A new method of measuring aerosol optical properties from digital twilight photographs**

M. Saito and H. Iwabuchi

with those from the skyradiometer measurements, and this comparison showed consistency between the results, with a coefficient of determination as large as 0.86. A case study for three different atmospheric conditions was presented to demonstrate the usefulness of the method. Comparison with products provided by other instruments and results from other model was used to investigate the effects of vertical inhomogeneity for aerosol species and profiles in detail. This investigation showed that AOTs can be retrieved with reasonable accuracy without knowing the details of such properties.

The difficulty in retrieving the coarse–fine particle volume ratio  $\zeta$  can be explained by the following. In cases with a large AOT, the following are true: the sensitivity of  $\zeta$  in twilight sky is weak, and retrieval uncertainty for  $\tau_{st}$  may lead to errors in  $\zeta$  retrievals. In cases with a small AOT, one possible explanation is that polarization effects cause non-negligible differences between the twilight sky brightness and color as found by the forward model simulations and that found by measurement. The forward model uses a scalar approximation to model the radiative transfer. Saito et al. (2013) investigated the contribution of multiply scattered light to twilight sky near the horizon with the JACOSPAR RTM, from which the present forward model is descended. The fraction of multiply scattered light is in the range of 20 to 50 % near the horizon for a VZA of 90–85° under small AOT conditions ( $0.05 < \tau_{tr} < 0.13$ ). Mishchenko et al. (2006) demonstrated that scalar approximation leads to biases for calculated radiance, with the magnitude of the bias in the range of  $\pm 3$ –5 % depending on the RAA, relative to the vector RTM outputs for AOTs of 0.1–0.3. This may cause an error in the retrieved brightness and color in twilight near the horizon. Another possible reason is the seeming insensitivity of  $\zeta$  in twilight sky when looking near the horizon (with SZA of  $\sim 90^\circ$ ), and this sensitivity may be too low to overcome the uncertainties resulting from model errors and camera noise. An investigation of this possibility and improvements to the algorithm to compensate are left for future work.

The retrieval method proposed by this paper can be applied to aerosol measurements in desert, snow-covered, and polar regions, areas where it is difficult to apply the conventional solar reflection-based methods. Particularly in the polar region in winter,

Title Page

Abstract

Introduction

Conclusions

References

Tables

Figures

◀

▶

◀

▶

Back

Close

Full Screen / Esc

Printer-friendly Version

Interactive Discussion



## A new method of measuring aerosol optical properties from digital twilight photographs

M. Saito and H. Iwabuchi

Title Page

Abstract

Introduction

Conclusions

References

Tables

Figures

◀

▶

◀

▶

Back

Close

Full Screen / Esc

Printer-friendly Version

Interactive Discussion



aerosol measurements are very limited, and the present twilight photometry method should be useful to increase the availability of aerosol measurements. Furthermore, it is easy to extend the aerosol observations at many points with this method because of the use of a digital camera, which is both inexpensive and easily movable. Digital cameras are widely used in daily life, and many amateur photographers have the opportunity to take pictures of beautiful sights, including twilight sky. In addition to their beauty, twilight photographs have the potential to be used as measurement data for aerosol retrievals. Therefore, the present aerosol retrieval method has unique characteristics, and it may complementarily be used in combination with other measurement techniques.

*Acknowledgements.* The authors are grateful to Mitsumu Ejiri of the National Institute of Polar Research and Isao Murata of Tohoku University for their assistance in the development of camera measurement techniques and to Toshihiko Takemura of Kyushu University for providing SPRINTARS data. We also thank SKYNET for the use of skyradiometer data in this research and the OpenCLASTR project for the use of the RSTAR package to calculate radiative transfer. This study was partly supported by a Grant-in-Aid for Scientific Research (DC1 262947) from the Japan Society for the Promotion of Science (JSPS).

## References

- Adams, C. N., Plass, G. N., and Kattawar, G. W.: The influence of ozone and aerosols on the brightness and color of the twilight sky, *J. Atmos. Sci.*, 31, 1662–1674, 1974.
- Berkoff, T. A., Sorokin, M., Stone, T., Eck, T. F., Hoff, R., Welton, E., and Holben, B.: Nocturnal aerosol optical depth measurements with a small-aperture automated photometer using the moon as a light source, *J. Atmos. Ocean. Tech.*, 28, 1297–1306, 2011.
- Bohren, C. F. and Huffman, D. R.: *Absorption and Scattering of Light by Small Particles*, John Wiley & Sons, New York, 2008.
- Bourassa, A. E., Degenstein, D. A., Gattinger, R. L., and Llewellyn, E. J.: Stratospheric aerosol retrieval with optical spectrograph and infrared imaging system limb scatter measurements, *J. Geophys. Res.*, 112, D10217, doi:10.1029/2006JD008079, 2007.

## A new method of measuring aerosol optical properties from digital twilight photographs

M. Saito and H. Iwabuchi

Title Page

Abstract

Introduction

Conclusions

References

Tables

Figures

◀

▶

◀

▶

Back

Close

Full Screen / Esc

Printer-friendly Version

Interactive Discussion



- Dave, J. V. and Mateer, C. L.: The effect of stratospheric dust on the color of the twilight sky, *J. Geophys. Res.*, 73, 6897–6913, 1968.
- Dubovik, O., Holben, B., Eck, T. F., Smirnov, A., Kaufman, Y. J., King, Y. J., Tanre, D., and Slutsker, I.: Variability of absorption and optical properties of key aerosol types observed in worldwide locations, *J. Atmos. Sci.*, 59, 590–608, 2002.
- Ehrlich, A., Bierwirth, E., Wendisch, M., Herber, A., and Gayet, J.-F.: Airborne hyperspectral observations of surface and cloud directional reflectivity using a commercial digital camera, *Atmos. Chem. Phys.*, 12, 3493–3510, doi:10.5194/acp-12-3493-2012, 2012.
- Hänel, G.: The properties of atmospheric aerosol particles as functions of the relative humidity at thermodynamic equilibrium with the surrounding moist air, *Adv. Geophys.*, 19, 73–188, 1976.
- Hayasaka, T., Nakajima, T., Ohta, S., and Tanaka, M.: Optical and chemical properties of urban aerosols in Sendai and Sapporo, Japan, *Atmos. Environ.*, 26, 2055–2062, 1992.
- Herber, A., Thomason, L. W., Gernandt, H., Leiterer, U., Nagel, D., Schulz, K. H., Kaptur, J., Albrecht, T., and Notholt, J.: Continuous day and night aerosol optical depth observations in the Arctic between 1991 and 1999, *J. Geophys. Res.*, 107, 4097, doi:10.1029/2001JD000536, 2002.
- Hess, M., Koepke, P., and Schult, I.: Optical properties of aerosols and clouds: the software package OPAC, *B. Am. Meteorol. Soc.*, 79, 831–844, 1998.
- Hioki, S. and Iwabuchi, H.: Photographic observation and optical simulation of a pollen corona display in Japan, *Appl. Opt.*, 54, B12–B21, 2015.
- Holben, B. N., Eck, T. F., Slutsker, I., Tanré, D., Buis, J. P., Setzer, A., Vermote, E., Reagan, J. A., Kaufman, Y. J., Nakajima, T., Lavenu, F., Jankowiak, I., and Smirnov A.: AERONET – a federated instrument network and data archive for aerosol characterization, *Remote Sens. Environ.*, 66, 1–16, 1998.
- Hulburt, E. O.: Explanation of the brightness and color of the sky, particularly the twilight sky, *J. Opt. Soc. Am.*, 43, 113–118, 1953.
- Intergovernmental Panel on Climate Change (IPCC): Climate Change 2013: The Physical Science Basis, Contribution of Working Group I to the Fifth Assessment Report of the IPCC, edited by: Stocker, T. F., Qin, D., Plattner, G. K., Tignor, M., Allen, S. K., Boschung, J., Nauels, A., Xia, Y., Bex, V., and Midgley, P. M., Cambridge University Press, Cambridge, UK, New York, NY, USA, 2013.

## A new method of measuring aerosol optical properties from digital twilight photographs

M. Saito and H. Iwabuchi

Title Page

Abstract

Introduction

Conclusions

References

Tables

Figures

◀

▶

◀

▶

Back

Close

Full Screen / Esc

Printer-friendly Version

Interactive Discussion



- Iwabuchi, H. and Suzuki, T.: Multiple-scaling method for anisotropic scattering and its applications to radiance calculations, *AIP Conf. Proc.*, 41, 1100, doi:10.1063/1.3117009, 2009.
- Iwabuchi, H., Yamada, S., Katagiri, S., Yang, P., and Okamoto, H.: Radiative and microphysical properties of cirrus cloud inferred from the infrared measurements made by the Moderate Resolution Imaging Spectroradiometer (MODIS). Part I: Retrieval method, *J. Appl. Meteorol. Clim.*, 53, 1297–1316, 2014.
- Kataoka, R., Miyoshi, Y., Shigematsu, K., Hampton, D., Mori, Y., Kubo, T., Yamashita, A., Tanaka, M., Takahei, T., Nakai, T., Miyahara, H., and Shiokawa, K.: Stereoscopic determination of all-sky altitude map of aurora using two ground-based Nikon DSLR cameras, *Ann. Geophys.*, 31, 1543–1548, doi:10.5194/angeo-31-1543-2013, 2013.
- Lee Jr., R. L. and Andres, J. H.: Measuring and modeling twilight's purple light, *Appl. Optics*, 42, 445–457, 2003.
- Lee Jr., R. L., Meyer, W., and Hoeppe, G.: Atmospheric ozone and colors of the Antarctic twilight sky, *Appl. Optics*, 50, 162–171, 2011.
- Llewellyn, E. J., Lloyd, N. D., Degenstein, D. A., Gattinger, R. L., Petelina, S. V., Bourassa, A. E., Wiensz, J. T., Ivanov, E. V., McDade, I. C., Solheim, B. H., McConnell, J. C., Haley, C. S., von Savigny, C., Sioris, C. E., McLinden, C. A., Griffioen, E., Kaminski, J., Evans, W. F. J., Puckrin, E., Strong, K., Wehrle, V., Hum, R. H., Kendall, D. J. W., Matsushita, J., Murtagh, D. P., Brohede, S., Stegman, J., Witt, G., Barnes, G., Payne, W. F., Piché, L., Smith, K., Warshaw, G., Deslauniers, D. -L., Marchand, P., Richardson, E. H., King, R. A., Wevers, I., McCreath, W., Kyrölä, E., Oikarinen, L., Leppelmeier, G. W., Auvinen, H., Mégie, G., Hauchecorne, A., Lefèvre, F., de La Noë, J., Ricaud, P., Frisk, U., Sjöberg, F., von Schéele, F., and Nordh, L.: The OSIRIS instruments on the Odin spacecraft, *Can. J. Phys.*, 82, 411–422, 2004.
- Mateshvili, N., Fussen, D., Mateshvili, G., Mateshvili, I., Vanhellemont, F., Kyrölä, E., Tukiainen, S., Kujanpää, J., Bingen, C., Robert, C., Tétard, C., and Dekemper, E.: Nabro volcano aerosol in the stratosphere over Georgia, South Caucasus from ground-based spectrometry of twilight sky brightness, *Atmos. Meas. Tech.*, 6, 2563–2576, doi:10.5194/amt-6-2563-2013, 2013.
- Minnaert, M. G. J.: *Light and Color in the Outdoors*, vol. 17, Springer Verlag, 1993.
- Mishchenko, M. I., Travis, L. D., and Lacis, A. A.: *Multiple Scattering of Light by Particles: Radiative Transfer and Coherent Backscattering*, Cambridge Univ. Press, New York, 2006.
- Murtagh, D., Frisk, U., Merino, F., Ridal, M., Jonsson, A., Stegman, J., Witt, G., Eriksson, P., Jiménez, C., Megie, G., de la Noë, J., Ricaud, P., Baron, P., Pardo, J. R., Hauchcorne, A.,



## A new method of measuring aerosol optical properties from digital twilight photographs

M. Saito and H. Iwabuchi

Title Page

Abstract

Introduction

Conclusions

References

Tables

Figures

◀

▶

◀

▶

Back

Close

Full Screen / Esc

Printer-friendly Version

Interactive Discussion



Takemura, T., Okamoto, H., Maruyama, Y., Numaguchi, A., Higurashi, A., and Nakajima, T.: Global three-dimensional simulation of aerosol optical thickness distribution of various origins, *J. Geophys. Res.*, 105, 17853–17873, 2000.

5 Takemura, T., Nakajima, T., Dubovik, O., Holben, B. N., and Kinne, S.: Single-scattering albedo and radiative forcing of various aerosol species with a global three-dimensional model, *J. Climate*, 15, 333–352, 2002.

Takemura, T., Nozawa, T., Emori, S., Nakajima, T. Y., and Nakajima, T.: Simulation of climate response to aerosol direct and indirect effects with aerosol transport-radiation model, *J. Geophys. Res.*, 110, D02202, doi:10.1029/2004JD005029, 2005.

10 Volz, F. E.: Twilight phenomena caused by the eruption of Agung volcano, *Science*, 144, 1121–1122, 1964.

Volz, F. E.: Note on the global variation of stratospheric turbidity since the eruption of Agung volcano, *Tellus*, 4, 513–515, 1965.

15 Watts, P. D., Bennartz, R., and Fell, F.: Retrieval of two-layer cloud properties from multispectral observations using optimal estimation, *J. Geophys. Res.*, 116, D16203, doi:10.1029/2011JD015883, 2011.

Wu, B. and Lu, D.: Retrieval of stratospheric background aerosol scattering coefficient from twilight polarization measurements, *Appl. Optics*, 27, 4889–4906, 1988.

20 Zhou, L., Dickinson, E., Tian, Y., Zeng, X., Dai, Y., Yang, Z. -L., Schaaf, C. B., Gao, F., Jin, Y., Strahle, A., Myneni, B., Yu, H., Wu, W., and Shaikh, M.: Comparison of seasonal and spatial variations of albedos from Moderate-resolution Imaging Spectroradiometer (MODIS) and Common Land Model, *J. Geophys. Res.*, 108, 4488, doi:10.1029/2002JD003326, 2003.

## A new method of measuring aerosol optical properties from digital twilight photographs

M. Saito and H. Iwabuchi

**Table 1.** Camera equipment characteristics.

Equipment	Period of observation	Coordinates	ISO	f-stop
Nikon D7000 equipped with a fish-eye lens	Jan 2013 to Aug 2014	Sendai, Japan (38°15′ N, 140°50′ E)	200	f2.8

Title Page

Abstract

Introduction

Conclusions

References

Tables

Figures

◀

▶

◀

▶

Back

Close

Full Screen / Esc

Printer-friendly Version

Interactive Discussion



## A new method of measuring aerosol optical properties from digital twilight photographs

M. Saito and H. Iwabuchi

**Table 2.** Viewing and solar directions used for aerosol retrievals.

Direction	Angles [°]
Viewing zenith angles (VZA)	60, 70, 75, 80, 82, 84, 85, 86, 87, 88
Relative azimuth angles (RAA)	0, 10, 20, 30
Solar zenith angles (SZA)	90, 91, 92, 93, 94, 95, 96

Title Page

Abstract

Introduction

Conclusions

References

Tables

Figures

◀

▶

◀

▶

Back

Close

Full Screen / Esc

Printer-friendly Version

Interactive Discussion



## A new method of measuring aerosol optical properties from digital twilight photographs

M. Saito and H. Iwabuchi

**Table 3.** Parameters for the aerosol vertical profile assumed in the forward model.

Vertical profile	$\xi$	$\psi$
Background $b_{bg}$	1	1
Boundary layer $b_{bl}$	2	1
Upper layer $b_{up}$	5	0.8
Stratosphere $b_{st}$	12	1.5

Title Page

Abstract

Introduction

Conclusions

References

Tables

Figures

◀

▶

◀

▶

Back

Close

Full Screen / Esc

Printer-friendly Version

Interactive Discussion



## A new method of measuring aerosol optical properties from digital twilight photographs

M. Saito and H. Iwabuchi

**Table 4.** Prior information and its error range for the state vector elements.

Variable	$x$	$x_a$	Geometric SD	Min	Max
Tropospheric AOT	$\ln \tau_{tr}$	$\ln 0.13$	1.19	$\ln 0.01$	$\ln 0.5$
Stratospheric AOT	$\ln \tau_{st}$	$\ln 0.1$	1.15	$\ln 0.002$	$\ln 0.1$
Coarse–fine particle volume ratio	$\ln \zeta$	$\ln 1.08$	2.3 (= $\ln 10$ )	$\ln 0.2$	$\ln 5$

Title Page

Abstract

Introduction

Conclusions

References

Tables

Figures

◀

▶

◀

▶

Back

Close

Full Screen / Esc

Printer-friendly Version

Interactive Discussion



## A new method of measuring aerosol optical properties from digital twilight photographs

M. Saito and H. Iwabuchi

**Table 5.** Reference values and variabilities assumed for error analysis.

Error source	Variable	Assumed value	Assumed variability ( $\sigma$ )
Measurement error	$\mathbf{y}$	–	Defined by $\mathbf{S}_{y,m}$
Forward model approximation	As above	–	Defined by $\mathbf{S}_{y,\text{fwd}}$
Model parameters	$\ln \omega_{\text{H}_2\text{O}}$	$8.62 \text{ kg m}^{-2}$	$2.58 < \omega_{\text{H}_2\text{O}} < 25.8 \text{ kg m}^{-2}$
	$\omega_{\text{O}_3}$	321 DU	$280 < \omega_{\text{O}_3} < 360 \text{ DU}$
	$m_r$	1.5	$1.44 < m_r < 1.57$
	$\ln m_i$	0.01	$0.001 < m_i < 0.1$
	$\ln \alpha$	0.1	$0.05 < \alpha < 0.3$

Title Page

Abstract

Introduction

Conclusions

References

Tables

Figures

◀

▶

◀

▶

Back

Close

Full Screen / Esc

Printer-friendly Version

Interactive Discussion

## A new method of measuring aerosol optical properties from digital twilight photographs

M. Saito and H. Iwabuchi

**Table 6.** Retrieval results and SPRINTARS model simulation results for case studies.

Date	Retrievals					SPRINTARS AOT	
	Camera		Skyrad		Sunpho	Sulfate	Dust
	AOT	$\zeta$	AOT	$\zeta$	AOT		
(a) 31 Jan 2013, morning	$0.074 \pm 0.012$	$2.86 \pm 0.34$	0.108	1.116	0.083	0–0.02	0–0.02
(b) 23 May 2013, morning	$0.101 \pm 0.006$	$0.98 \pm 0.07$	0.112	1.193	0.122	0.03–0.05	0.1–0.2
(c) 3 Jun 2013, morning	$0.251 \pm 0.006$	NA	0.296	1.366	0.311	0.03–0.05	0.1–0.2

NA: not available

Title Page

Abstract

Introduction

Conclusions

References

Tables

Figures

◀

▶

◀

▶

Back

Close

Full Screen / Esc

Printer-friendly Version

Interactive Discussion



# AMTD

8, 191–234, 2015

## A new method of measuring aerosol optical properties from digital twilight photographs

M. Saito and H. Iwabuchi

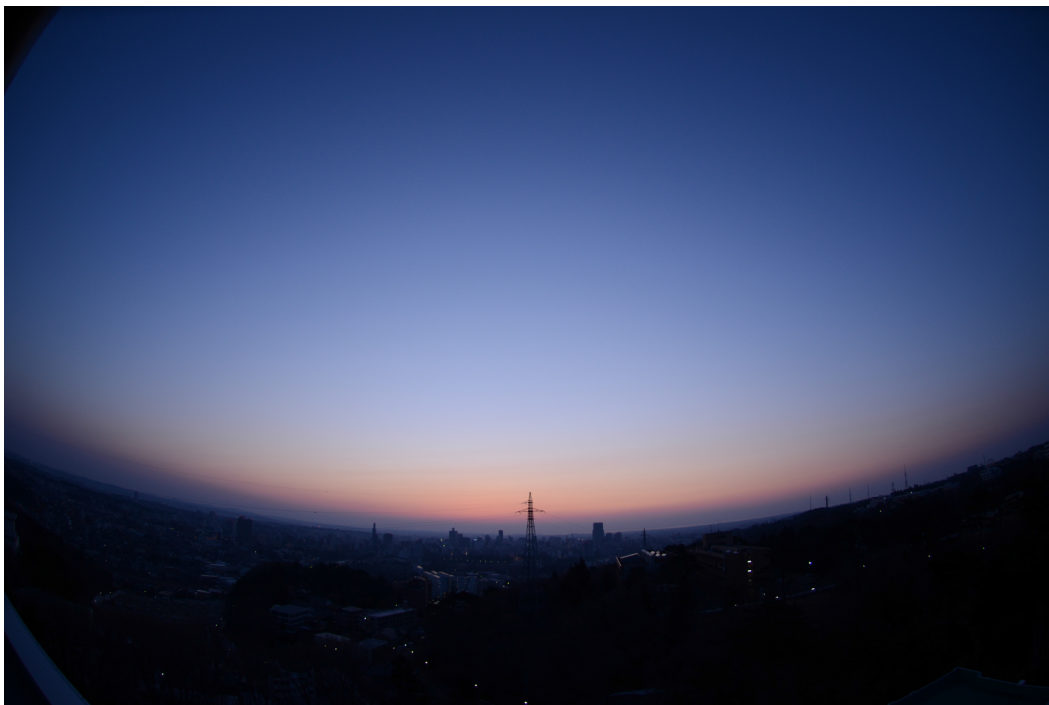


**Figure 1.** An example of a twilight sky photograph taken on 23 March 2012 in the morning.

Title Page

Abstract

Introduction

Conclusions

References

Tables

Figures

◀

▶

◀

▶

Back

Close

Full Screen / Esc

Printer-friendly Version

Interactive Discussion



## A new method of measuring aerosol optical properties from digital twilight photographs

M. Saito and H. Iwabuchi

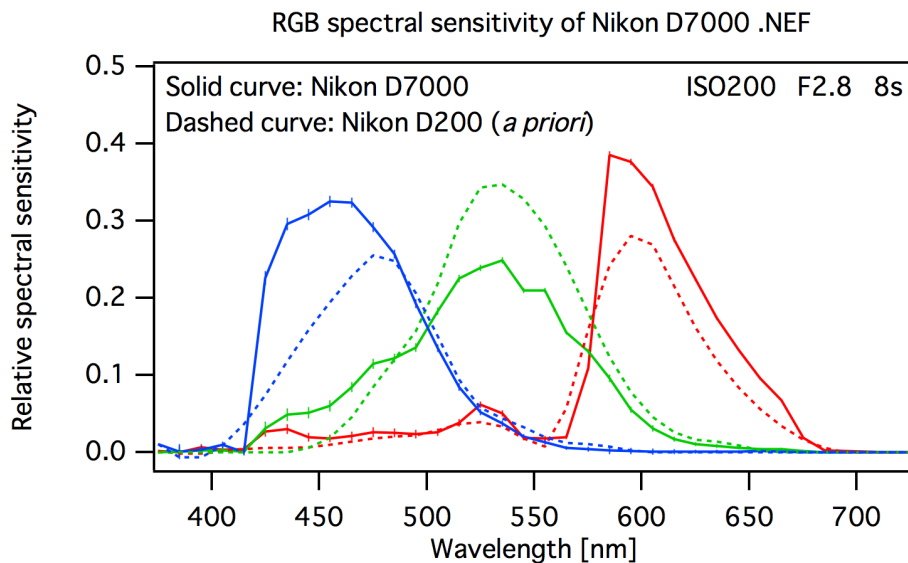


**Figure 2.** Inferred color-matching functions of Nikon D7000 in this study (solid lines) and of D200 (dotted lines) from Sigarnes et al. (2008).

Title Page

Abstract

Introduction

Conclusions

References

Tables

Figures

◀

▶

◀

▶

Back

Close

Full Screen / Esc

Printer-friendly Version

Interactive Discussion



## A new method of measuring aerosol optical properties from digital twilight photographs

M. Saito and H. Iwabuchi

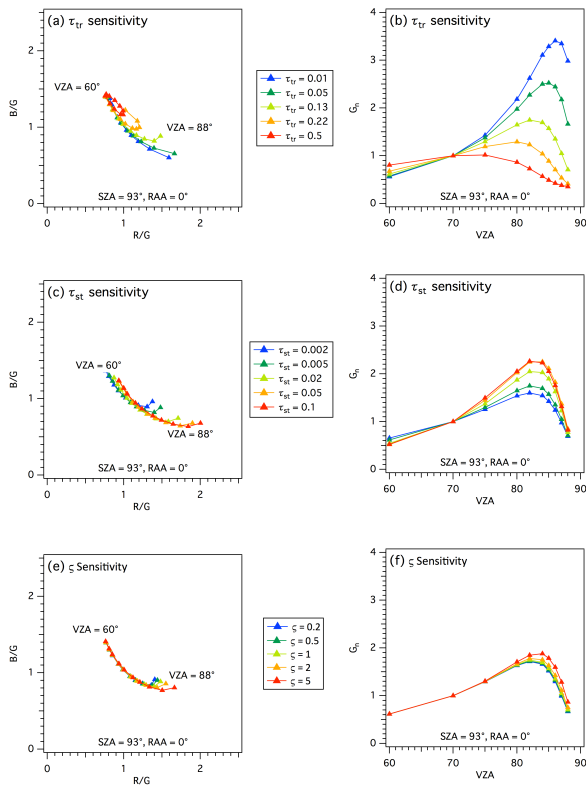


**Figure 3.** Sensitivity test results for normalized brightness ( $G_n$ ) and chromaticity ( $B/G$ ,  $R/G$ ) of twilight sky: **(a, b)** sensitivities to tropospheric aerosol optical thickness; **(c, d)** sensitivity to stratospheric aerosol optical thickness; **(e, f)** sensitivity to coarse–fine particle volume ratio. Panels on the right side **(b, d, f)** show the dependence of normalized brightness variations along with the viewing zenith angles. Panels on the left side **(a, c, e)** show the dependence of chromaticity variations along with the viewing zenith angles on  $R/G$ – $B/G$  cross sections. SZA and RAA are  $93$  and  $0^\circ$ , respectively.

Title Page	
Abstract	Introduction
Conclusions	References
Tables	Figures
◀	▶
◀	▶
Back	Close
Full Screen / Esc	
Printer-friendly Version	
Interactive Discussion	



## A new method of measuring aerosol optical properties from digital twilight photographs

M. Saito and H. Iwabuchi

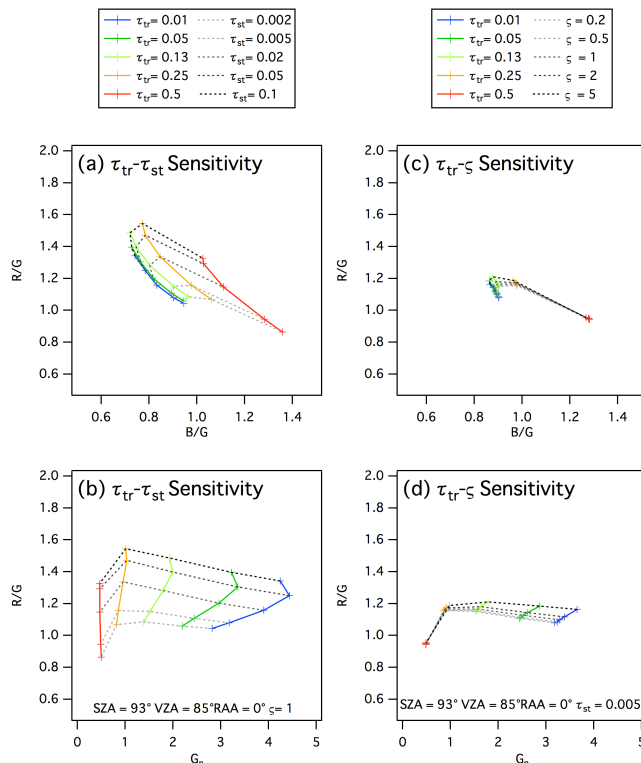


**Figure 4.** Sensitivity test results for chromaticity values of the twilight glow (VZA of 85° and SZA of 93° at the solar azimuth angle): **(a, b)** show the dependence of chromaticity variations on the R/G–B/G cross section; **(c, d)** show the dependence of normalized brightness variations on the R/G– $G_n$  cross section. Dashed curves in the panels on the right **(b, d)** are isolines of coarse–fine particle volume ratio, and solid curves are isolines of tropospheric aerosol optical thickness. Dashed curves in the panels on the left **(a, c)** are isolines of stratospheric aerosol optical thickness, and solid curves are isolines of tropospheric aerosol optical thickness.

Title Page

Abstract Introduction

Conclusions References

Tables Figures

◀ ▶

◀ ▶

Back Close

Full Screen / Esc

Printer-friendly Version

Interactive Discussion

## A new method of measuring aerosol optical properties from digital twilight photographs

M. Saito and H. Iwabuchi

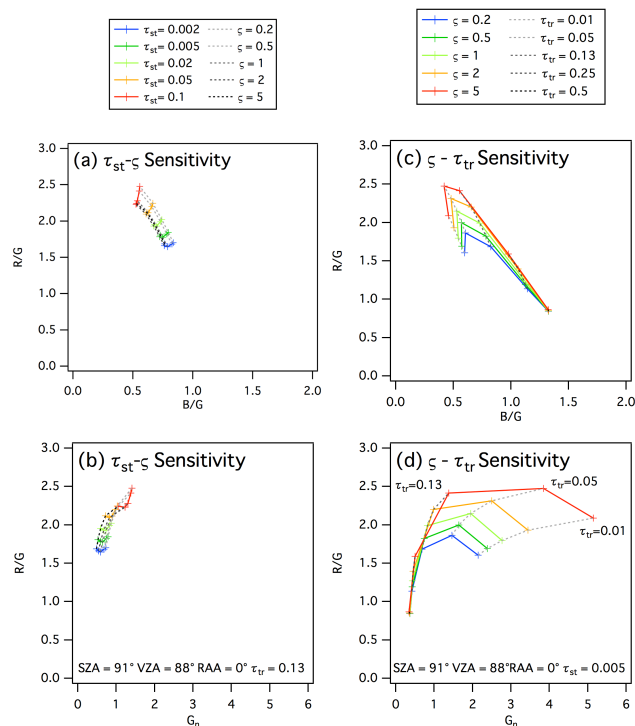


**Figure 5.** Sensitivity test results for chromaticity values of the twilight sky near the horizon (VZA of 88° and SZA of 91° at the solar azimuth angle): **(a, b)** show the dependence of chromaticity variations on the R/G–B/G cross section; **(c, d)** show the dependence of normalized brightness variations on the R/G–G<sub>n</sub> cross section. Dashed curves in the panels on the right **(b, d)** are isolines of tropospheric aerosol optical thickness, and solid curves are isolines of coarse–fine particle volume ratio. Dashed curves in the panels on the left **(a, c)** are isolines of coarse–fine particle volume ratio, and solid curves are isolines of stratospheric aerosol optical thickness.

## A new method of measuring aerosol optical properties from digital twilight photographs

M. Saito and H. Iwabuchi

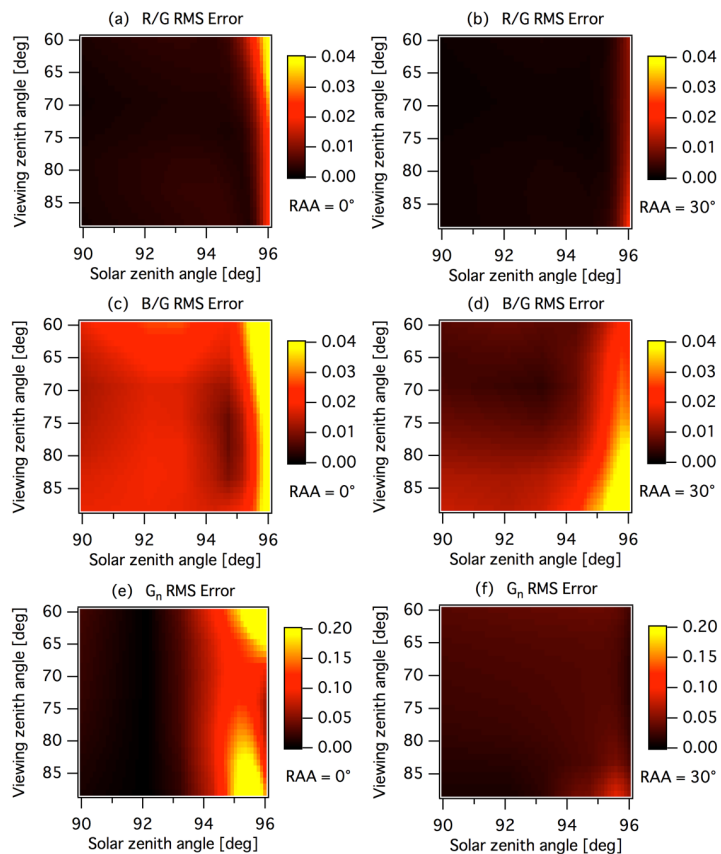


**Figure 6.** Forward model errors in **(a, b)** R/G, **(c, d)** B/G, and **(e, f)**  $G_n$  caused by the model assumptions as functions of SZA and VZA (see text for details). Panels on the left **(a, c, e)** have RAA = 0°, and those on the right **(b, d, f)** have RAA = 30°.

Title Page

Abstract

Introduction

Conclusions

References

Tables

Figures

◀

▶

◀

▶

Back

Close

Full Screen / Esc

Printer-friendly Version

Interactive Discussion

## A new method of measuring aerosol optical properties from digital twilight photographs

M. Saito and H. Iwabuchi

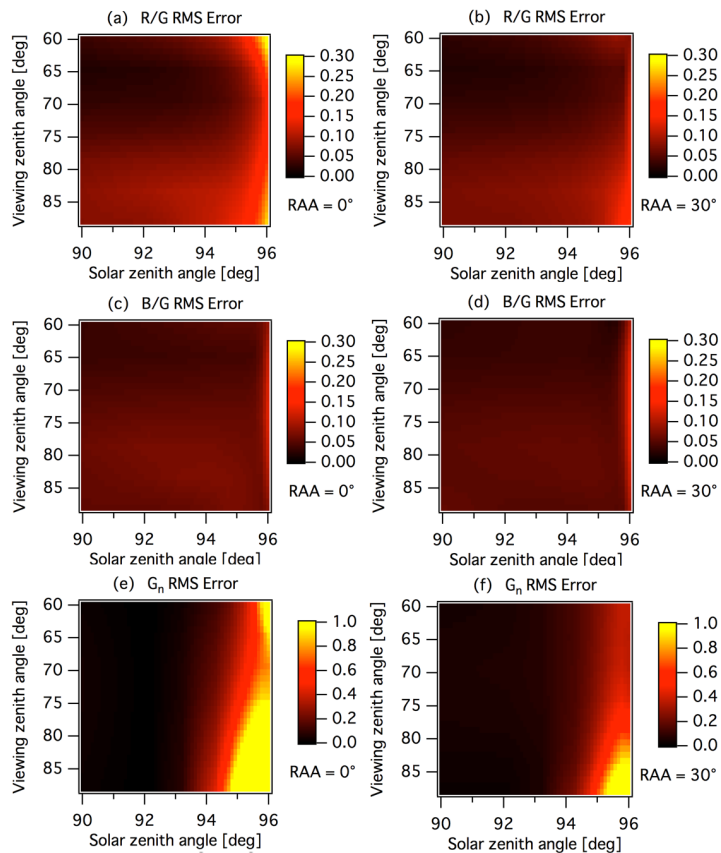


**Figure 7.** Forward model errors in **(a, b)** R/G, **(c, d)** B/G, and **(e, f)**  $G_n$  caused by uncertainties in the model parameters as functions of SZA and VZA. Panels on the left **(a, c, e)** have RAA =  $0^\circ$ , and those on the right have RAA =  $30^\circ$ .

[Title Page](#)
[Abstract](#)
[Introduction](#)
[Conclusions](#)
[References](#)
[Tables](#)
[Figures](#)
[◀](#)
[▶](#)
[◀](#)
[▶](#)
[Back](#)
[Close](#)
[Full Screen / Esc](#)
[Printer-friendly Version](#)
[Interactive Discussion](#)

## A new method of measuring aerosol optical properties from digital twilight photographs

M. Saito and H. Iwabuchi

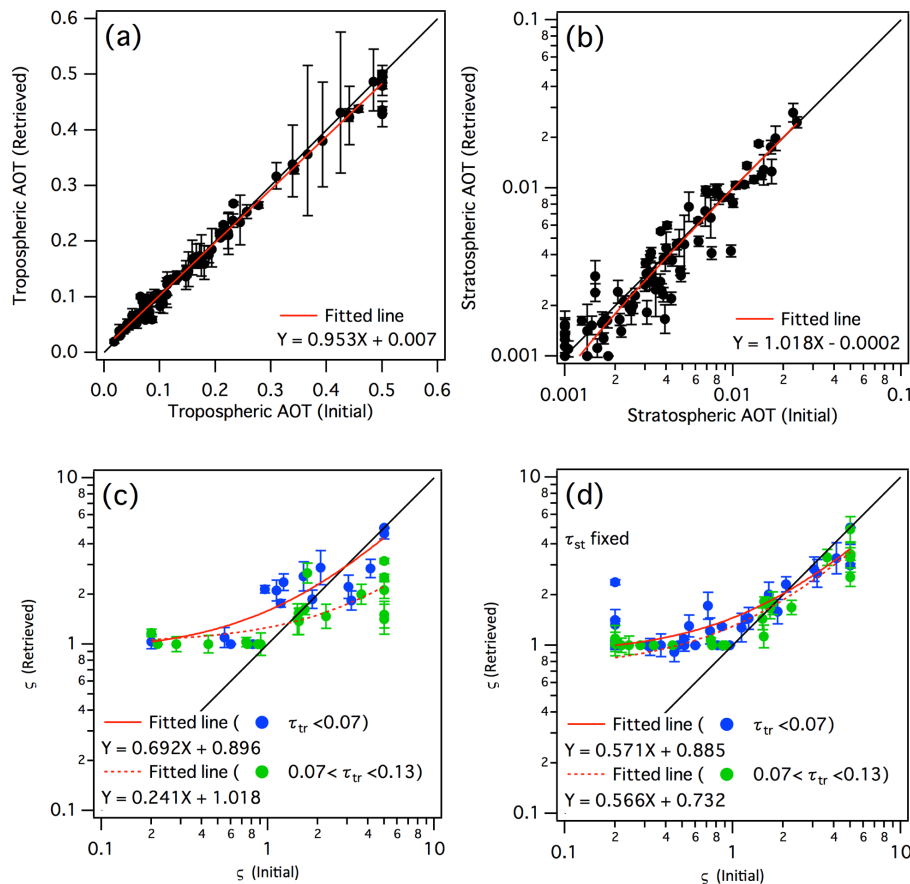


**Figure 8.** Initial and retrieved (a) tropospheric aerosol optical thickness, (b) stratospheric aerosol optical thickness, and (c) coarse–fine particle volume ratio  $\zeta$  in the retrieval-error analysis. (d) Same as (c) but retrievals under fixed stratospheric aerosol optical thickness. Blue and green marks show  $\zeta$  retrievals under very and moderately clean conditions, respectively.

Title Page	
Abstract	Introduction
Conclusions	References
Tables	Figures
◀	▶
◀	▶
Back	Close
Full Screen / Esc	
Printer-friendly Version	
Interactive Discussion	

## A new method of measuring aerosol optical properties from digital twilight photographs

M. Saito and H. Iwabuchi

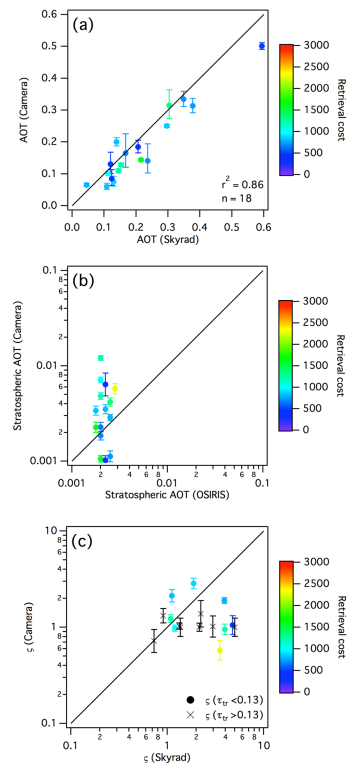


**Figure 9.** Comparison of aerosol property retrievals from camera measurements and skyradiometer measurements. Error bars show uncertainty of retrievals. Color scales show total retrieval cost  $J(\mathbf{x})$ . The vertical axis and horizontal axis show retrievals from a camera and those from other instruments, respectively: **(a)** aerosol optical thickness, from camera and skyradiometer, with coefficient of determination  $r^2$  at 0.86 and 18 trials; **(b)** stratospheric aerosol optical thickness, from camera and OSIRIS onboard the Odin satellite; **(c)** coarse–fine particle volume ratio, from camera and skyradiometer, with black X marks indicating retrievals in dense aerosol conditions ( $\tau_{tr} > 0.13$ ).

## A new method of measuring aerosol optical properties from digital twilight photographs

M. Saito and H. Iwabuchi

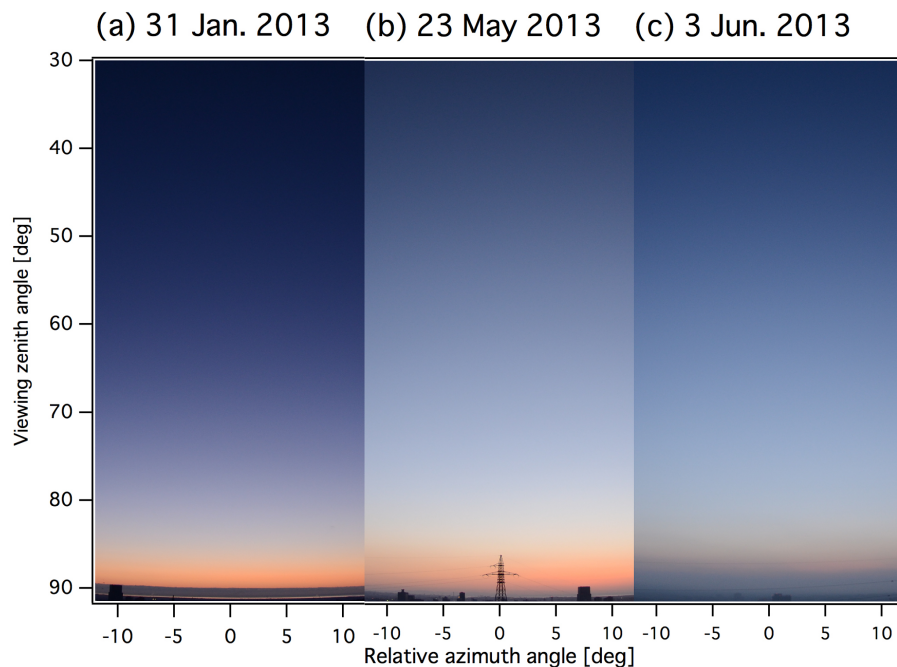


**Figure 10.** Photographs of twilight sky on the solar side, for the case studies of **(a)** 31 January 2013, **(b)** 23 May 2013, and **(c)** 3 June 2013. In all cases, SZA is uniformly  $94^\circ$ , and VZA is  $90.45^\circ$  at the horizon,  $91.5^\circ$  at the bottoms of the images, and  $30^\circ$  at the tops of the photographs.

Title Page

Abstract

Introduction

Conclusions

References

Tables

Figures

◀

▶

◀

▶

Back

Close

Full Screen / Esc

Printer-friendly Version

Interactive Discussion



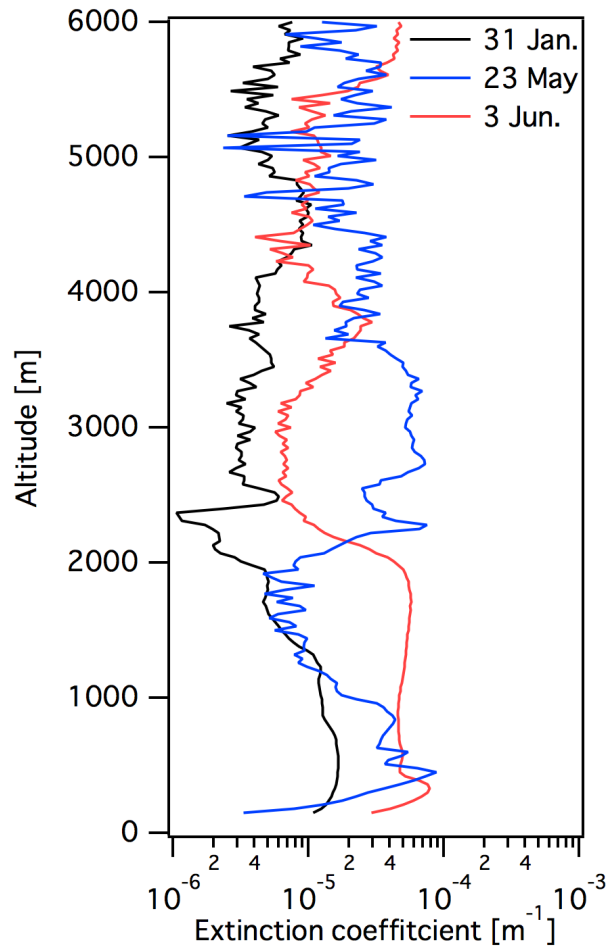


**Figure 11.** Vertical profiles of aerosol extinction coefficients for altitudes from 0 to 6 km, as obtained from lidar measurements for the case studies. Data for 0 to 150 m are not available.

## A new method of measuring aerosol optical properties from digital twilight photographs

M. Saito and H. Iwabuchi

Title Page

Abstract

Introduction

Conclusions

References

Tables

Figures

◀

▶

◀

▶

Back

Close

Full Screen / Esc

Printer-friendly Version

Interactive Discussion

